ELSEVIER

International Journal of Solids and Structures 41 (2004) 413–434

INTERNATIONAL JOURNAL OF SOLIDS and STRUCTURES

www.elsevier.com/locate/ijsolstr

The stress–elongation relation for an adhesive layer loaded in peel using equilibrium of energetic forces

T. Andersson, U. Stigh *

Department of Engineering Science, University of Skövde, P.O. Box 408, SE-541 28 Skövde, Sweden

Received 21 March 2003; received in revised form 22 September 2003

Abstract

An experimental method to determine the stress–elongation relation for a thin adhesive layer loaded in peel is presented. The method is based on equilibrium of the energetic forces acting on a DCB-specimen. These energetic forces are identified to be associated with the geometrical positions of the acting loads and the start of the adhesive layer. The first energetic force is shown to be given by the product of the force and the rotation of the loading point. The second energetic force is shown to be given by the area under the stress–elongation curve for the adhesive layer. Using equilibrium of these energetic forces, the shape of the stress–elongation curve is determined. A test set-up is developed to facilitate the experiments. Special consideration is given to the accuracy of the measurement of the elongation of the adhesive. Results from two sets of experiments with slightly varying geometry are presented. The main result is that the stress–elongation relation can be described by a curve divided into three parts; initially the stress increases proportionally to the elongation. This corresponds to a linear elastic behaviour of the layer. The next part is given by a constant limiting stress. The curve ends with a parabolically softening part. After this point, a crack has been initiated in the adhesive. The experimental results are first compared to an asymptotic analysis using linear elastic fracture mechanics. This shows that the new method to evaluate the fracture energy gives consistent results. The experiments are also simulated using the measured stress–elongation law. Good agreement with the experiments is achieved which further validates the method. The fracture energy and the maximum peel stress are found to agree well within each set of experiments. Some variation is found between the two sets. This is accredited to differences in fracture initiation.

Keywords: Adhesive layer; Stress–elongation relation; *J*-integral; Experimental method

1. Introduction

During recent years, the automobile industry has shown an increasing interest in adhesive joining. It has been recognised that the torsional rigidity and the fatigue strength of a car can be substantially increased if the conventional spot welds are complemented with adhesive bonding. Adhesive joining is also a technique that works well when introducing un-conventional materials such as composites and aluminium alloys in

* Corresponding author. Tel.: +46-500-448508; fax: +46-500-448599.
E-mail address: ulf.stigh@ite.his.se (U. Stigh).

0020-7683/$ - see front matter © 2003 Elsevier Ltd. All rights reserved.
doi:10.1016/j.ijsolstr.2003.09.039

the production. However, modern design methods are critically dependent on accurate constitutive models to facilitate simulation of the structure early in the design process. There is therefore a need for good material models and data for the numerical methods. These are, however, not easy to determine for thin adhesive layers.

An alternative to constitutive modelling is the use of fracture mechanics. The success of this method is critically dependent on the possibility to disregard the actual fracture processes taking place in the adhesive. To this end, the process zone should be embedded in a "simply" parameterised stress field. The *parameters* then control the fracture process in the sense that the same parameters that give crack growth for one structure also give crack growth for any other structure. In small scale yielding (SSY) the size of the process zone shall be much smaller than any other length scale. This condition can be formulated as in the ASTM condition.

$$l > 2.5\left(\frac{K_{\mathrm{Ic}}}{\sigma_{\mathrm{Y}}}\right)^2 = 2.5\frac{G_{\mathrm{c}}E'}{\sigma_{\mathrm{Y}}^2} \tag{1}$$

where l is the smallest characteristic length scale of the problem, and K_{Ic}, σ_{Y} and G_{c} are the fracture toughness, the yield strength and the fracture energy of the adhesive, respectively. Moreover, $E' = E$ for plane stress and $E/(1-\nu^2)$ for plane strain; E and ν are Young's modulus and Poisson's ratio, respectively. In most cases l is either the thickness of the adhesive layer or the length of a preexisting crack. With a typical adhesive layer thickness of only a fraction of a millimeter, the condition is too severe. Thus, SSY is not applicable for most structural adhesives. Moreover, it is well known that the fracture energy and morphology varies with the thickness of the adhesive layer (cf. e.g. Chai, 1988). It has also proven very hard to correlate the bulk properties of adhesives with their behaviour in a thin and constrained layer (cf. e.g. Adams et al., 1978; Adams and Coppendale, 1979; Xia and Hutchinson, 1994). However, simplified analyses of adhesive joints based on through-thickness averages of stress and strain have often proven successful. The basic variables are then the peel stress, σ, the shear stress, τ, the elongation, w, and the shear deformation, v, of the adhesive *layer*, cf. Fig. 1. In order to emphasize that the adhesive layer is treated as a structural entity in this class of methods, we propose to name it the *adhesive layer theory*. For the case of a thin and soft adhesive layer, the use of this theory is motivated by an asymptotic expansion analysis by Klarbring (1991). Thus, for the development of engineering methods it appears more fruitful to use an "adhesive layer" approach to the problem.

If the deformation gradient along the adhesive layer is zero then the state of the adhesive is homogeneous apart from small regions at the free boundaries of the layer. With a brittle adhesive, fracture is expected to be governed by the details of the state at these boundaries. With a ductile adhesive, the fields are smeared

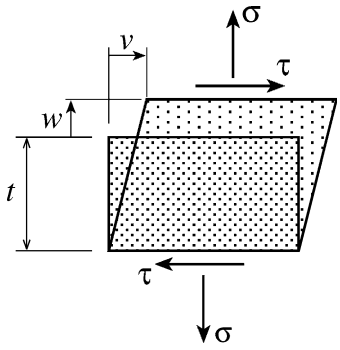

Fig. 1. Basic deformation modes of an adhesive layer with thickness t. Conjugated stress and deformation measures are (w, σ) for peel and (v, τ) for shear.

out and fracture can be predicted by the average stress. This is indicated in the experiments by cf. e.g. Adams et al. (1978) and Adams and Coppendale (1979). Thus, the use of σ, τ, w, and v as basic variables is well motivated. With a small gradient along the adhesive layer, the approach should still be applicable, cf. the notch sensitivity results by Sørensen (2002). A criteria for the validity of the adhesive layer theory is that the process zone shall be large compared to the thickness of the layer. Otherwise, the gradients through the thickness of the layer should be taken into consideration. Now, if the process zone is small compared to the remaining relevant length scales but large as compared to the layer thickness, the fracture process is adequately modelled using only one parameter of the loading. This is usually chosen as the energy release rate, J. On the other hand, with a process zone that is large compared to the layer thickness and other relevant length scales, a complete constitutive description is needed.

The adhesive layer theory is well suited for use with the finite element method (cf. Stigh, 1987, 1988; Edlund, 1992; Wernersson and Gustafsson, 1987; Yang et al., 1999, 2001a,b; Sørensen, 2002). A constitutive law can be formulated in terms of σ, τ, w, v and a number of internal variables to model the non-elastic development of the layer under stress. A framework for development of the law is given by Alfredsson and Stigh (2003). In order to develop the law it is necessary to know the behaviour of the layer in simple load cases. To this end Olsson and Stigh (1989) theoretically solved an inverse problem for the DCB-specimen, cf. Fig. 2. That is, given the elongation w of the adhesive layer at its start, the applied force $F(w)$, and the rotation of the loading point $\theta(w)$, the stress–elongation relation is given by

$$\sigma(w) = \frac{2}{b}\frac{\mathrm{d}(F\theta)}{\mathrm{d}w} \tag{2}$$

where b is the width of the specimen. This formula was derived based on the Euler–Bernoulli theory for elastic beams and assuming the existence of a functional relation $\sigma(w)$. An experimental method and some preliminary experimental results are reported by Stigh and Andersson (2000). A critical examination of the criteria for a valid measurement is given by Andersson and Stigh (2001).

Recently, similar approaches have been presented. Sørensen (2002) use a DCB-specimen loaded with bending moments M. In this case the J-integral can be measured continuously during an experiment through

$$J(w) = 12(1-\nu^2)\frac{M(w)^2}{B^2H^3E} \tag{3}$$

where B is the width, H the height and E Young's modulus of the adherends. Using

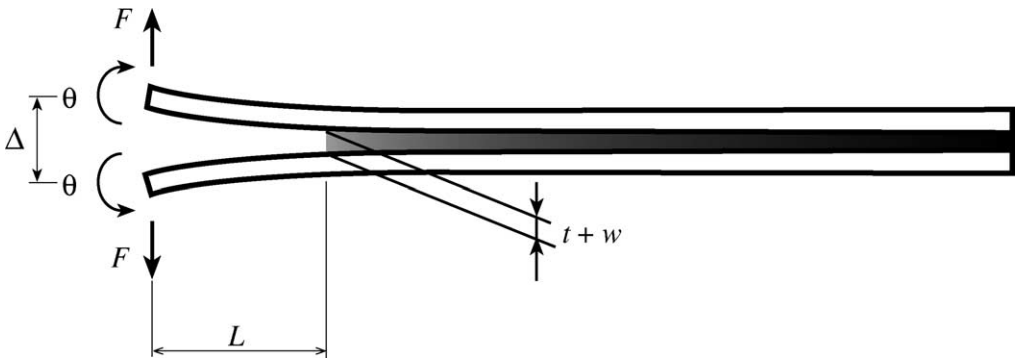

Fig. 2. DCB-specimen with measured quantities F, θ, Δ and w.

$$\sigma(w) = \frac{\mathrm{d}J(w)}{\mathrm{d}w} \tag{4}$$

and simultaneous measurement of w yields $\sigma(w)$. It can be noted that the same approach is taken by Sørensen and Jacobsen (1998), Jacobsen and Sørensen (2001) and Fernberg and Berglund (2001) in measurements of the bridging law for composites. The main drawback with this approach, as compared to the present, is that the details of the adherends are involved in Eq. (3). Thus, a number of extra measurements need to be made, i.e. the geometry and the elastic modulus of the adherends. Especially the geometrical parameters greatly affect the quality of the measurements through the powers two and three in the equation.

Another approach to the problem of determining the stress–deformation relation is presented by Yang et al. (1999, 2001a,b). The constitutive behaviour is described by the ad hoc stress–elongation law of Fig. 3. This law is characterised by the work of separation per unit area of crack advance, Γ_0 (equal to the area under the stress–elongation curve) the peak stress, σ_0 and two shape parameters δ_1/δ_c and δ_2/δ_c, cf. Fig. 3. Yang et al. (1999, 2001a,b) perform both experiments and numerical analyses on test specimens where the adherends are exposed to large plastic strains. By fitting the numerical results to the experiments the parameters Γ_0 and σ_0 are determined. The remaining two parameters are considered less important and they are chosen as $\delta_1/\delta_c = 0.15$ and $\delta_2/\delta_c = 0.5$. Using the same parameters on a different geometry, they capture, both qualitatively and quantitatively, the characteristics of the experiments. In variance with this method, the present experimental method does not require an a priori defined constitutive law with free parameters to be determined.

The underlying theory for the determination of the σ–w curve for the DCB-specimen is derived in the following section.

2. Theory

In an attempt to derive the field equations of elasticity similarly as the field equations of elastostatics, Eshelby (1951) introduced the concept of the *energetic force* associated with an object in an elastostatic field. For planar problems, with x_α denoting the Cartesian components of the position vector of an object, the Cartesian components J_α of the energetic force is defined by

$$J_\alpha \equiv -\frac{\partial \Pi}{\partial x_\alpha} \tag{5}$$

where Π denotes the potential energy per unit width of the body, i.e. the sum of the strain energy of the body and the potential energy of the prescribed forces acting on the body. The form of Eq. (5) immediately

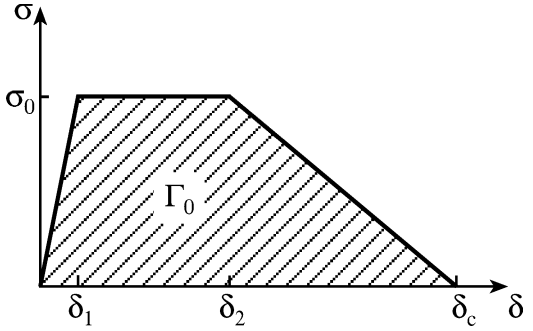

Fig. 3. Stress–elongation law used by Yang et al. (1999, 2001a,b).

implies the meanings of the notion of *object* and the concept of *equilibrium of energetic forces*. All features of a body and its loading that alters the potential energy of the body when they are moved are to be considered as *objects* in this respect. For instance, if the motion of a boundary of a body alters the potential energy, then the boundary is an object and an energetic force is associated with it. If all objects are considered, the simultaneous motion of them by the same amount will move the body and its loading as a rigid body. Hence, it will not change the potential energy. Thus, the sum of all energetic forces is zero, i.e. equilibrium in the conventional sense prevails for energetic forces. It should be recognised that the material must be elastic, or at least, *act* as if it is elastic. This is a critical requirement in the present application and it will be checked carefully. If the material deforms non-elastically, the concept of energetic forces still applies if the material never experiences reversed loading from a non-elastically deformed state. Moreover, if the material is elastically homogeneous in the ξ_α direction then the energetic force in that direction can be calculated from the path independent integral

$$J_\alpha \equiv \int_S (W n_\alpha - T_\gamma u_{\gamma,\alpha})\,\mathrm{d}S \tag{6}$$

Here, n_α is the outward normal to the path S enclosing the object, $T_\gamma = \sigma_{\gamma\alpha} n_\alpha$ is the traction vector and $W \equiv \int \sigma_{\alpha\beta}\,\mathrm{d}\epsilon_{\alpha\beta}$ is the strain energy density.

Considering the equilibrium of the energetic forces acting in the horizontal direction on the DCB-specimen of Fig. 2 it is immediately recognised that the potential energy is given by the positions of the two forces and the position of the start of the adhesive layer. The other conceivable objects, i.e. the left and right boundaries of the specimen are unloaded if the specimen is long enough. Thus, altering their positions will leave the potential energy constant. Denoting the horizontal components of the energetic forces associated with the two forces J_F and the energetic force associated with the start of the adhesive layer J_a, equilibrium requires

$$J_\mathrm{a} + 2J_\mathrm{F} = 0 \tag{7}$$

Thus, it remains to determine J_a and J_F.

In order to determine J_a consider an integration path A to B according to Fig. 4. Consistent with the assumed deformation modes of the adhesive layer, cf. Fig. 1, we will now assume that the boundary A to B is a vertical straight line. Along this line the traction vector T_γ is zero, thus the horizontal component of Eq. (6) becomes

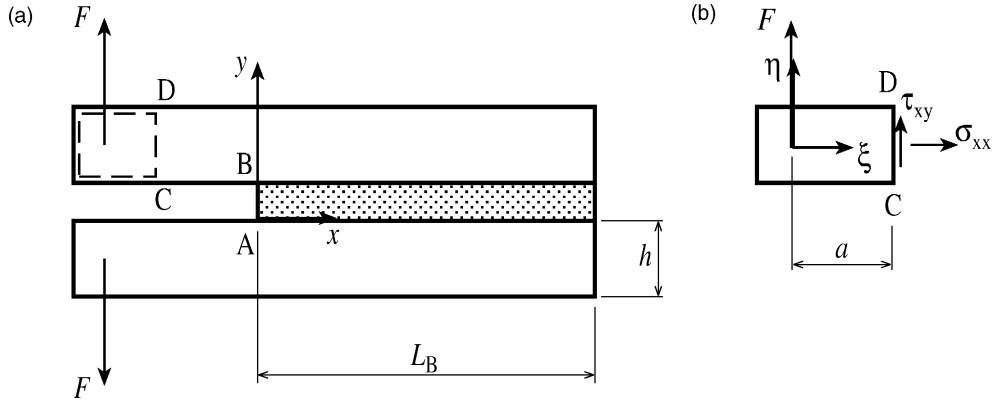

Fig. 4. (a) DCB-specimen with indicated integration paths. (b) Free-body diagram over integration path for the force.

$$J_a = \int_0^t W \, dy \tag{8}$$

Here and subsequently, the coordinate systems and symbols defined in Fig. 4 are used. Along AB, the only non-zero stress component is the peel stress σ. If we assume, consistently with the assumed deformations modes, that the strain is constant through the thickness, we arrive at

$$J_a = \int_0^t \left[\frac{1}{t} \int_0^w \sigma(\tilde{w}) \, d\tilde{w} \right] dy = \int_0^w \sigma(\tilde{w}) \, d\tilde{w} \tag{9}$$

Next, the J-integral is applied to the contour that incorporates the upper force F, cf. Fig. 4. The only path contributing to J_F is the path CD. The strain energy density is $W = (1/2)\sigma_{xx}\epsilon_{xx}$ since the shear strain is zero in the Euler–Bernoulli beam theory. According to the theory

$$\sigma_{xx} = -\frac{F\xi}{I_b}\eta, \quad \epsilon_{xx} = \frac{\sigma_{xx}}{E}, \quad \tau_{xy} = -\frac{3F}{2bh}\left(1 - 4\frac{\eta^2}{h^2}\right) \tag{10}$$

with $I_b = bh^3/12$. With the rotation $\partial v/\partial x = -\theta(\xi)$, insertion in Eq. (6) yields

$$J_F = -\frac{F^2\xi^2}{2bEI_b} - \frac{F\theta(\xi)}{b} = -\frac{F}{b}[\varphi(\xi) + \theta(\xi)] \tag{11}$$

where the rotation $\varphi(\xi) = F\xi^2/2EI_b$ is introduced. The right hand side now appears to be a function of ξ. However, the J-integral is path independent and shall not depend on ξ. This is indeed the case which can be shown by determining the J-integral for two different paths

$$\begin{aligned} &\xi \to 0: \; J_F(F,0) = -F\theta(0)/b \\ &\xi = a: \; J_F(F,a) = -F[\varphi(a) + \theta(a)]/b \end{aligned} \tag{12}$$

Taking the difference yields

$$J_F(F,a) - J_F(F,0) = -\frac{F}{b}[\theta(0) - \varphi(a) - \theta(a)] \tag{13}$$

which equals zero since $\theta(0) = \varphi(a) + \theta(a)$ according to the beam theory. Thus, the path independence is retained and

$$J_F = -\frac{F\theta}{b} \tag{14}$$

A similar derivation performed on a path surrounding the lower force F gives the same result.

Using the concept of equilibrium of energetic forces, cf. Eq. (7), we can now write

$$\int_0^w \sigma(\tilde{w}) \, d\tilde{w} = \frac{2F\theta}{b} \tag{15}$$

Differentiation yields Eq. (2).

3. Experimental set-up, specimens and adhesive

An experiment consists of a gradual separation of the loading points and a simultaneous measurement of F, θ and w. Multiplying F with θ and divide by b gives J_F according to Eq. (14). In order to find the σ–w curve, the product $F\theta$ is differentiated with respect to w according to Eq. (2). However, numerical differentiation of discretely measured data involves calculating the difference of quantities of nearly equal

magnitude impaired with measurement errors. Thus, the errors add up and may destroy the accuracy. In the design of the test equipment the accuracy of the transducers are of utmost importance. Stigh and Andersson (2000) report Monte-Carlo simulations of the experiments. These simulations are facilitated by an exact solution of the beam-equation-formulation of the DCB-problem with a saw-tooth formed σ–w curve (cf. Stigh, 1988). The simulations show that the measurement of the elongation of the adhesive must be performed with extra care, especially since the present adhesive (Ciba-Geigy XW1044-3) [1] show a fracture strain of only about 5% in uniaxial tension. Moreover, Wernersson and Gustafsson (1987) report an elastic part of the σ–w curve of about 10–30% of the entire curve for wood adhesives. Considering these results, the expected elastic part of the curve is about 1–3 μm. This clearly indicates that a very sensitive measurement method should be used. The chosen method is an interferometric strain/displacement method (ISDG) developed by Sharpe (1989). Here a brief description is given. For details see Sharpe (1989).

3.1. Measurement of the elongation of the adhesive

Two Vicker indentations are made on each adherend at the start of the adhesive layer, cf. Fig. 5. The indentations have four planar surfaces that act as small mirrors; the size c is typically 50–60 μm. These indentations are illuminated with a laser. Due to the shape of the indentations, the laser beam is reflected ($\phi = 44°$) in four directions. As a result, four diffraction patterns become visible. Due to the difference in path length between the planes of the indentations and the detection plane, interference patterns become visible inside the diffraction patterns.

By following the position, m, of a fringe it is possible to determine the elongation w. Elementary optics gives

$$\Delta w = \frac{\lambda}{\sin\phi}\Delta m \tag{16}$$

The total elongation is given by $w = \sum \Delta w$. The factor $\lambda/\sin\phi$ is 0.911 μm in this case using a laser with the wavelength $\lambda = 632.8$ nm. Hence, when a minimum has travelled one position, i.e. $\Delta m = 1$, the adhesive has elongated 0.911 μm. The interference pattern is recorded using two CCD-cameras, cf. Fig. 5. Two cameras are used to cancel out any rigid body translation of the specimen. The present CCD-cameras have 739×575 pixels in a rectangular area with the size 6.3×4.8 mm. Since the data processing is rather time consuming only 200 columns and 20 rows of the pixels are used in the experiments, cf. Fig. 6. Furthermore, in order to decrease the influence of disturbances in the interference pattern, the intensity of each column of pixels is summed up. This gives intensity curves according to Fig. 6.

By measuring the distance, ΔX, which a minimum has moved, Δm is determined from $\Delta m = \Delta X/X$, where X is the distance between two minima. The increment in w of the adhesive layer, between two measurements, is then given by Eq. (16).

In an experiment, it is appropriate to record five minima in the area of 200×20 pixels, cf. Fig. 6. The positions of three minima are followed in the evaluation of the interference patterns. The resolution of the w-measurement is estimated as follows; if three minima are followed there are roughly five fringe distances captured along the 200 pixels recorded by the CCD-camera. Hence, there are 40 pixels between two minima; a distance corresponding to 0.9 μm. Thus, one pixel corresponds to about 23 nm.

The actual accuracy of the w-measurement is difficult to determine. This is due to noise in the interference pattern that might produce false minima. These could easily be minimised using a "low pass filter". In effect, this is done by summing the intensity of light from the columns of pixels as described above. However, if the pattern contains too much noise it is possible that the process places the minima at

[1] Now renamed DOW BETAMATE XW1044-3.

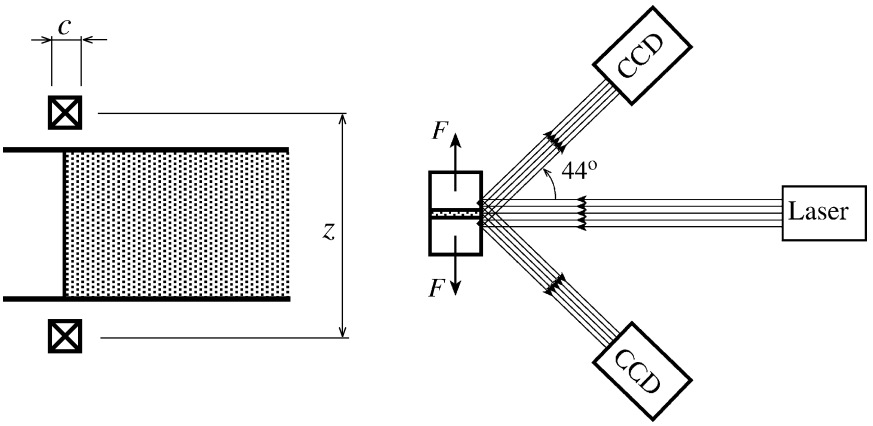

Fig. 5. Left: Two Vickers indentations placed on each adherend at the start of the adhesive layer. Right: Laser light reflected by the indentations giving interference patterns at positions of the CCD-cameras.

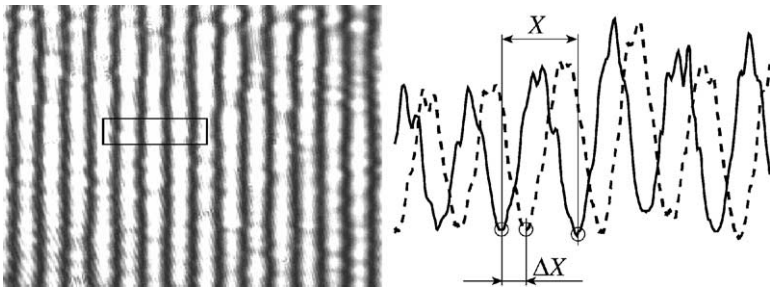

Fig. 6. Left: Interference pattern recorded in a CCD-camera. The pixels (20×200) that are used in the w-measurements are indicated with the rectangular area in the interference pattern. Right: Recorded pattern, calculated by summing the columns. The motions of the pattern is indicated by the dashed line.

incorrect positions, i.e. both X and ΔX might have large errors. Therefore it is of utmost importance that the surface preparation is carried out carefully. It should also be emphasised that in each experiment the w-measurement is evaluated manually.

The main drawback with the present system using CCD-cameras is that it is difficult to record fast processes, i.e. with increments of displacement larger than the distance between two minima (0.9 μm). Under these circumstances, the experiments may give false values. A way to speed up the process is to use a so-called linear diode array (cf. Sharpe, 1989). In the present system the time between two measurements is 0.5 s.

The angle ϕ is an additional source of error. This has not been considered here. A deviation in ϕ will occur if the penetration of the indentation is not made exactly perpendicular to the surface of the adherend. However, the influence is probably small since the specimens are thoroughly manufactured.

3.2. Tensile test machine

The test machine utilised in these experiments is shown in Fig. 7. It is manufactured by Swetest Instrument AB (model 168) and has a load capacity of 1000 N.

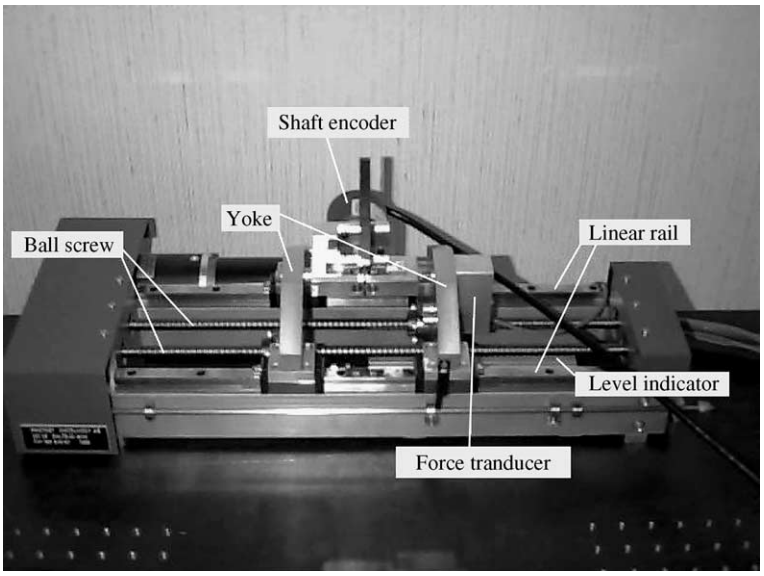

Fig. 7. Test machine.

During an experiment the yokes move away from each other symmetrically in relation to a midpoint between them, thus minimising any rigid body displacement of the specimen. The yokes slide along two linear rails. The movement is given by two ball screws, each rotating in opposite direction. If an ordinary tensile machine would be employed, the Vicker indentations might move out of the laser light. This would make it impossible to measure the elongation w. The clamping arrangement is shown in Fig. 8. The test specimen is attached to the yokes via the forks and the grips. Four ball bearings make it possible for the grips to rotate freely under loading thus minimising the applied bending moment at the loading points.

The force transducer is attached to one of the yokes. The right fork is connected to the force transducer through a hole in the same yoke. The shaft encoder is connected to the left yoke and moves with it. The shaft of the encoder is connected to the grips via a flexible coupling. Since the grips rotate with the test specimen, the rotation of the loading point, θ, is measured. A linear displacement transducer is used to measure the distance between the yokes. Due to the relatively stiff forks, it is reasonable to equate the distance between the yokes to the distance Δ between the applied forces.

3.3. Specimens and adhesive

Two different sets of specimens were manufactured. Set 1 contains five specimens and Set 2 four. Both sets are made of steel adherends with yield strength exceeding 470 MPa. The width of the adherends is nominally 5 mm for Set 1 and 4.5 mm for Set 2. However, each specimen is measured individually and the actual width is used in the evaluation of the experiments. The height of the adherends is 4.5 mm for Set 1 and 5 mm for Set 2. There are two substantial differences between the two sets of specimens. In Set 1 the free length L is 78 mm and in Set 2 L is 50 mm, cf. Fig. 2. Secondly, the glued length of the adhesive layer is 35 mm for Set 1 and 65 mm for Set 2. Moreover, the two sets were manufactured at different times using different steel alloys. The yield strength of the adherends is large enough to avoid any plastic deformation during the experiments. This is checked both numerically and visually after the specimen has fractured. The rate of separation, $\dot{\Delta}$, is about 0.009 m/s and is mainly limited by the time consuming w-measurement. The thickness of the adhesive layer is nominally 0.2 mm. Unfortunately, for Set 2 the thickness of the adhesive

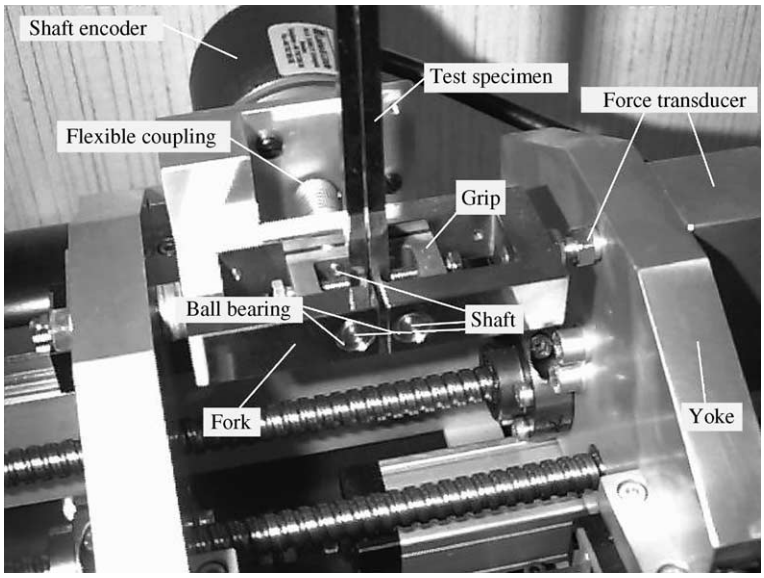

Fig. 8. Clamping arrangement.

layer is found to vary along the layer. The experiments of Set 2 are however evaluated in the same way as Set 1. Independent test results give the elastic modulus, the ultimate strength [2] and the fracture energy 2.22 GPa, 31.5 MPa, and 800 J/m^2, respectively.

4. Experimental results

Results within each set of experiments vary only slightly. However, some variation is observed between the two sets of experiments. Therefore, only one experiment from each set is presented here. All experimental results are presented elsewhere (cf. Andersson, 2002) and the results are summarised in Table 1. In this section, figures placed to the left are taken from Set 1, i.e. with the longer unbonded part; the figures to the right are from Set 2. The results are first checked against a simplified analysis based on linear elastic fracture mechanics (LEFM). Next, the J–w curves are presented and evaluated for the σ–w relation.

4.1. Comparison with LEFM

Fig. 9 shows load vs. separation of the loading points from two experiments. To check if the curves are reasonable, an asymptotic analysis based on linear elastic fracture mechanics is performed. This corresponds to a rigid-brittle adhesive layer, cf. the dashed curves in Fig. 9. The curve is divided into two parts corresponding to the phases prior to and after a crack starts to propagate. For a rigid-brittle adhesive layer, elementary beam theory gives the F–Δ curve

$$\Delta = \frac{2L^3}{3EI_b}F \tag{17}$$

[2] Strain rate = 0.02 min^{-1}.

Table 1
Geometrical data and constitutive parameters

Exp.	b (mm)	h (mm)	L (mm)	J_c (J/m^2)	w_1 (μm)	w_2 (μm)	w_3 (μm)	σ_0 (MPa)	Init.
2	4.9	4.5	78	930	1	8	80	26.7	co
4	4.9	4.5	77	800	1.6	7	85	24.3	co
5	5	4.5	78	770	1	8	71	24.5	co
6	5	4.5	79	730	0.5	5	77	28	co
7	4.9	4.5	76	890	2.7	6	113	22	ad
10	4.1	5	51	740	2	20	60	19.3	ad
11	4.4	5	50	670	3	20	50	19	ad
12	4.4	5	49	910	2.5	16	77	20.1	ad
14	4.4	5	48.5	740	2.4	14.5	84	20.6	ad

Experiments 2–7 are from Set 1; experiments 10–14 from Set 2. The last column indicates type of crack initiation where ad indicates adhesive fracture and co cohesive fracture, respectively.

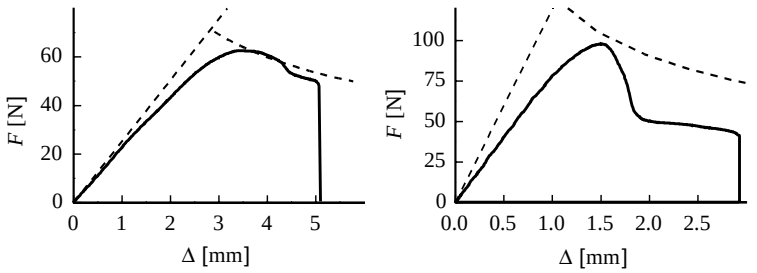

Fig. 9. Load vs. load point separation from two experiments. Left: Specimen from Set 1. Right: Specimen from Set 2. The solid lines are experimental data; dashed lines correspond to an asymptotic analysis based on linear elastic fracture mechanics.

where L is constant during the first phase of the experiment. This is the first part of the dashed curves. During the second phase, a crack propagates and consumes energy per unit crack area. The fracture energy is given by

$$J_c = \frac{F^2 L^2}{bEI_b} \tag{18}$$

where F and L vary simultaneously in order for J_c to remain constant during the second phase. Eliminating L from Eqs. (17) and (18) yields

$$F = \sqrt{\frac{A}{\Delta}} \tag{19}$$

where the constant A is given by $A \equiv b^2\sqrt{J_c^3 E h^3/27}$. This relation is shown in Fig. 9 as the descending dashed lines. The values of J_c are taken as the maximum values of J during the experiments, cf. Fig. 10. Except the value of L, geometrical data are taken as measured on the actual specimens. The value of L is set to the nominal value, 78 mm for Set 1 and 50 mm for Set 2. In the simulations we neglect the flexibility of the adhesive layer. As expected, the asymptotic curves in Fig. 9 lie above the experimental curves. It would be interesting to compare the location of the start of crack propagation in the experiments and the simulations. However, the interferometric method used to measure w made it necessary to make the experiments in a dark room. Thus, no visual inspection of the specimen was possible during the experiment. It should be noted that the initial stiffness is very sensitive to the geometrical data; both L and h are raised to the power

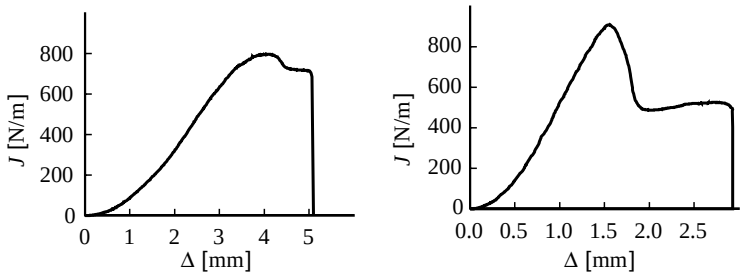

Fig. 10. J vs. Δ during two experiments. Left: Curve from Set 1. Right: Curve from Set 2.

three in the expression for the stiffness. Thus, small errors in these data substantially affect the result. Furthermore, the transducer used to measure Δ induces errors in the order of 3–5%.

The results in Fig. 9 also illustrates the discussion in the introduction on the use of fracture mechanics. For many engineering applications the prediction of the behaviour of a DCB-like structures given by the dashed lines in Fig. 9 is adequate. For these cases, only one parameter for the adhesive layer is necessary, namely J_c.

4.2. Evaluation of the J-curves

Fig. 10 shows the J-integral vs. the separation of the loading points, Δ. The curves are monotonically increasing up to a value of approximately 800 N/m. Inspection of the fracture surfaces of the specimens shows that for all except one of the specimens of Set 1 fracture initiates cohesively, i.e. inside the adhesive layer. All specimens of Set 2 initially fracture adhesively, i.e. in the interface between the adhesive and the adherend. This explains the difference in J_c between the two sets.

After the maximum point, the curves are descending. According to the adhesive layer theory, J should remain constant during crack propagation. Instead, the experiments show a decreasing value of J to an apparent steady state value J_{ss}. The values of J_{ss} are only marginally smaller than J_c for the experiments in Set 1; in Set 2 the differences are substantial, the decrease is almost 50% (cf. Andersson, 2002). A difference between the initiation and the propagation values of J is common in fracture mechanics. It is usually ascribed to plasticity of the material in the vicinity of the crack tip. In this case, one probable explanation is that the local state of stress alters due to the formation of a sharp crack in the adhesive layer. This explains some of the difference between J_{ss} and J_c. Moreover, the cracks initiating adhesively change direction after about 1 mm of crack propagation and the remaining crack propagation is cohesive. It is tempting to ascribe the large difference between J_{ss} and J_c to this change in crack path. However, the one experiment of Set 1 initially fracturing adhesively shows similar behaviour as the other experiments of Set 1, i.e. a small decrease of J. Thus, the change in crack path does not seem to be the major cause of the substantial decrease of J in Set 2. Visual inspections of the specimens in Set 2 show that the thickness of the adhesive layer is varying along the specimen. At the start and at the end, the adhesive layer has the specified thickness of 0.2 mm. However, after approximately 5–10 mm, from both ends of the bonded length, the layer is notably thinner. This explains the large difference between J_{ss} and J_c for Set 2.

4.3. Stress–elongation relation

Fig. 11 shows the applied load vs. the elongation of the adhesive. The curves appear smooth and regular. It is however not possible, with the present measurement system, to measure w larger than about 50 μm due to the problems described in Section 3.1. Therefore it is difficult to determine the complete σ–w curve from

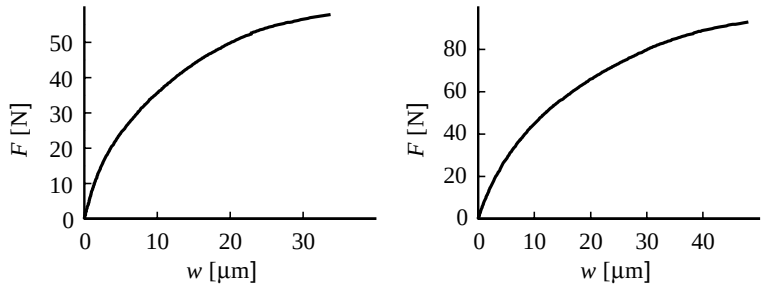

Fig. 11. Applied force vs. measured elongation of the adhesive layer. Left: Curve from Set 1. Right: Curve from Set 2.

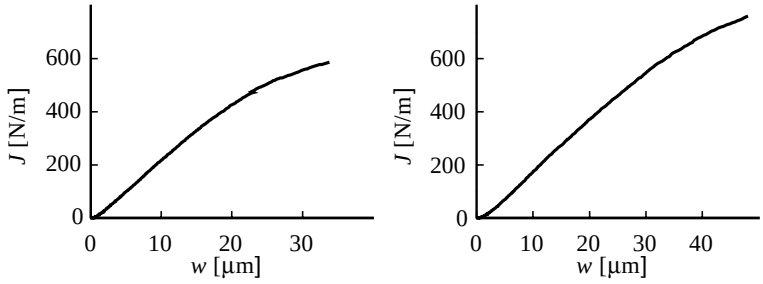

Fig. 12. Measured J vs. w. Left: Curve from Set 1. Right: Curve from Set 2.

these results. However, the maximum value of J, which is the area under the complete σ–w curve, is known, cf. Fig. 10. This value gives an important hint on the shape of the σ–w curve that is used in the sequel to determine the complete curve.

Fig. 12 shows typical J–w curves from the two sets. As shown, the curves are monotonically increasing until the measurement of w fails to give any more reliable data. The curves generally start with a convex part, followed by an approximately linear part. The curves end with a concave part.

For comparison, all the J–w curves are shown in the same graph in Fig. 13. There is a small scatter between most curves from Set 1. The exception is the one experiment which initially fractured adhesively which fits well to the curves of Set 2. The small scatter between the other curves in this set is attributed to noise in the interference patterns which gives rise to less accurate measurements of w. The results from Set 2 show less scatter. Most of these curves virtually coincide up to 30 μm indicating that the experiments are performed properly. Except for the one curve from Set 1 discussed above, all the curves from Set 1 are located above the ones from Set 2. This indicates that the specimens in Set 1 are stronger.

The most straightforward method to determine the σ–w curve from the experimental results is to differentiate the data. This inevitable results in large scatter in the σ–w curve since small errors in the measured data add up to give large errors after numerical differentiation. A better method is to use a series of functions to approximate the J–w curve and then differentiate the series. Following Fernberg and Berglund (2001) we use the series

$$\frac{J(w)}{J_c} = \sum_{i=1}^{n} A_i \exp\left(-\frac{nw}{iw_{ref}}\right) \tag{20}$$

where the parameters A_i are determined by the least square method. The parameters J_c and w_{ref} correspond to the maximum values of J and w recorded in the experiment. A typical result of a least square fit of

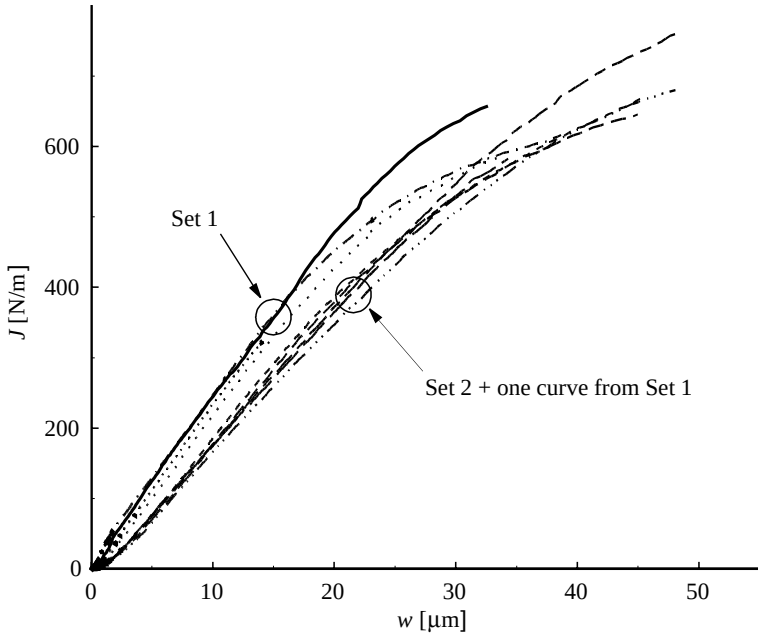

Fig. 13. Measured J vs. w from both sets.

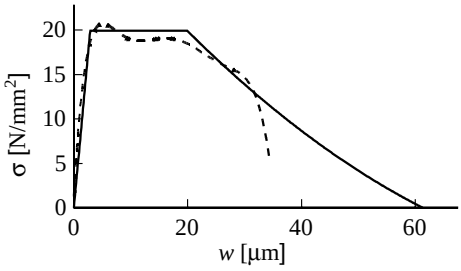

Fig. 14. σ–w. Dashed line: result from adjustment of Eq. (20). Solid line: result from adjustment of Eq. (21).

Eq. (20) to experimental data is shown in Fig. 14. As shown in the figure, the σ–w curve can roughly be divided into three parts; first a linearly increasing part corresponding to a linearly elastic response, then a plateau with a constant limiting stress and finally a descending part ending with zero stress and initiation of crack propagation.

4.4. Constitutive model

As explained above, the curves end at about 30 μm due to problems with the measurement of w. Thus, with limited knowledge of the descending part of the σ–w curve, we need some method to extrapolate the curve to $\sigma = 0$. The procedure used here is to divide the curve into three parts: one linearly increasing part, corresponding to a linear elastic response; one plateau; and finally, a parabolically descending part ending with fracture of the adhesive. Thus, the following σ–w curve is proposed

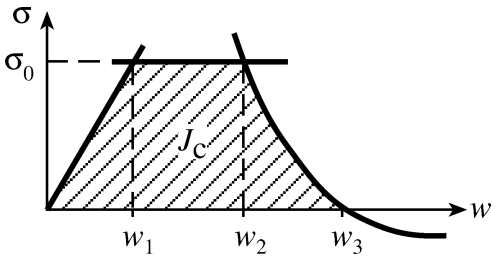

Fig. 15. σ–w curve based on Eq. (21) and the value of J_c.

$$\sigma(w) = \begin{cases} \sigma_0 w/w_1 & 0 \leqslant w < w_1 \\ \sigma_0 & w_1 \leqslant w < w_2 \\ aw^3 + bw + c & w_2 \leqslant w < w_3 \\ 0 & w_3 \leqslant w \end{cases} \tag{21}$$

The σ–w curve is illustrated in Fig. 15. The curve has five free parameters. However, we know that the area under the curve shall equal the maximal value of $J = J_c$. This decreases the number of free parameters and only four parameters remain to be adjusted to the experimental data.

The σ–w curve is thus parameterised using the four parameters σ_0, w_1, w_2 and w_3. Eq. (21) is first integrated and the four parameters are adjusted to the experimental J–w curve by minimising the quadratic error between the two curves. The resulting parameters are given in Table 1. Fig. 16 shows the experimental and the adjusted curve taken from one experiment in Set 2. The adjustment of the curves in Set 2 is generally better than those for Set 1.

All the adjusted σ–w curves are presented in Fig. 17a,b. Within each set, the curves appear fairly similar. However, there are two distinct differences between the two sets. The mean value of the maximum peel stress is 25 MPa for Set 1 and 20 MPa for Set 2. The mean value of the fracture energy is 820 J/m^2 for Set 1 and 760 J/m^2 for Set 2. There are at least two possible reasons for these discrepancies:

(1) The specimens in Set 2 have a lower interfacial strength which is manifested by the initial cohesive fracture. This is the most probable reason. If this is the case, the result demonstrates the importance of achieving a strong adhesion in the interface between the adhesive and the adherend.
(2) The two sets are manufactured at different times. The manufacturing process (curing time, etc.), inevitably induce residual stresses in the adhesive layer. These stresses are not easy to determine, but they

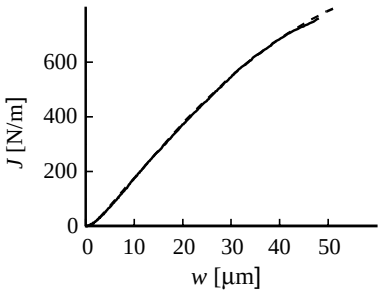

Fig. 16. Experimental and adjusted σ vs. w curve from Set 2. Solid line: experimental data. Dashed line: adjusted curve. Note that two curves are present in the graph.

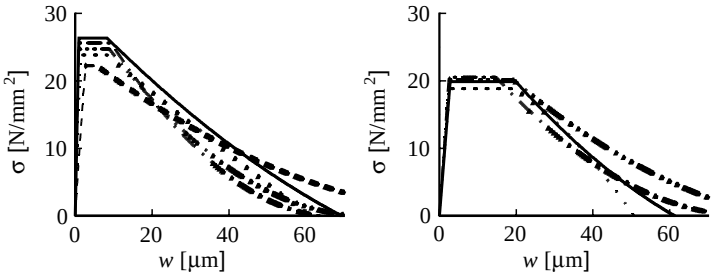

Fig. 17. (a) All adjusted σ vs. w curves from Set 1. (b) All adjusted σ vs. w curves from Set 2.

affect the apparent fracture energy (cf. Nairn, 2000). Unfortunately no information on the curing time is available.

Moreover, for the specimens in Set 2, the thickness of the adhesive layer is thinner in the middle of the specimen. If the adherends were planar before the adhesive bonding, this would result in compressive residual peel stresses at the start of the adhesive layer. This should give a stronger bond. However, the experiments show the reversed behaviour.

Bulk tests performed on the adhesive give a maximum tensile strength of about 30 MPa. Considering the high level of constraint, it is possible to assume a state of uniaxial strain in the present experiment instead of a state of uniaxial stress as in the bulk test. Using the von Mises criteria, the relation between the expected peel strength σ_0 and the yield strength σ_Y is given by

$$\sigma_0 = \frac{1-v}{1-2v}\sigma_Y \tag{22}$$

With $v = 0.4$ we would expect the maximum peel stress to be $\sigma_0 \approx 90$ MPa. This is 4 to 5 times larger than the measured one. [3] On a micromechanical level, the low value of σ_0 might be an effect of the local stress concentration at the bi-material corners between the adhesive and the adherends. This is probably an important factor in reducing the strength of the adhesive layer. However, the geometrical variations, on a micro scale, between the individual specimens are large and would suggest a larger scatter in peel strength than measured. Moreover, in many experiments the cracks do not appear to initiate at the interface. Another difference between the stress state in an adhesive layer and in a tensile test is the substantial difference in hydrostatic stress. In the elastic regime, with the present value of Poisson's ratio and with a specified peel/tensile stress, the hydrostatic stress is three times larger in the adhesive layer than in a tensile test. In the plastic regime, the strong constraint that the adherends exerts on the adhesive even enlarges this difference. The large hydrostatic stress might prove to be an important factor in explaining the low value of σ_0. On the structural mechanical length scale, implicit in the adhesive layer theory, the small value of σ_0 can be modelled as an effect of damage in the layer.

The maximum elongation of the adhesive layer is about 80 μm. This can be compared to ordinary bulk (tensile) tests that give a fracture strain of only about 5%. With the present thickness of the adhesive layer (0.2 mm) the corresponding elongation is 10 μm. This is only one eight of the measured value. Therefore, the critical strain measured in a uniaxial tensile test is inappropriate as a fracture criterion.

[3] It might be more appropriate to use a pressure modified von Mises criteria. However, the difference between the yield strength in compression and tension is too small to explain the present effect.

5. Validation of the experimental method

Contrary to ordinary experimental methods to determine the constitutive properties of a material, the present method utilizes a non-uniform state of stress and relies on the use of an inverse solution for the final determination of the properties of the adhesive layer. Certain requirements have to be met in order for the inverse solution to be valid. The critical requirements are:

(1) *Elastic behaviour of the adherends.* If the adherends develop plastic zones near the start of the adhesive layer, then these zones will contribute to increase J_F; this will disturb the measurements.
(2) *No reversed loading of the adhesive layer from an inelastically deformed state.* The J-value of the adhesive layer, Eq. (9), relies on a unique relation between the peel stress and the elongation of the adhesive layer. If the adhesive layer deforms inelastically a unique relation is still valid as long as unloading does not take place during the experiment.
(3) *Valid measurement of the elongation of the adhesive layer.* The adherends will deform anticlastically due to the bending moment. However, the elongation is measured at the surface of the adherends. Thus, the elongation at the centre of the adhesive layer will be somewhat larger than at the surface. This effect should be negligible for the measurement to be valid.
(4) *Sufficiency of a local theory for the behaviour of the adhesive layer.* This point is related to the second point above. The peel stress is assumed to depend on the local elongation of the adhesive layer, this is of course a simplification; not only the local elongation of the adhesive layer between two neighbouring points at the adherends determines the peel stress at these points, also the deformation in a neighbourhood of these points influence the representative stress.

The first requirement is easily checked by means of the experimental results. Considering the maximum force and the unbonded length L together with the geometry of the adherend, the maximum beam bending stress is about 370 MPa for the experiments in Set 1 and 270 MPa for Set 2. This should be compared to the yield strength that is larger than 470 MPa for the present alloy. It can be concluded that the adherends deform elastically. This is also verified by visual inspection of the specimens after the experiment.

The influence of anticlastic bending, requirement 3, is studied using elementary beam bending theory (cf. e.g. Timoshenko and Goodier, 1970). Since the peel stress is small, its influence on the deformation of the adherends is neglected. The cross section of the lower beam is shown in Fig. 18. The vertical displacement v is given by

$$v(y,z) = -\nu_b \frac{y^2 - z^2}{2R} \tag{23}$$

where R is the radius of curvature of the beam given by $R = EI_b/M = EI_b/FL$ and ν_b is Poisson's ratio for the adherends. The difference between v at the surface and at the interior is then given by

$$\eta(F(w)) \equiv v\left(-\frac{h}{2},\frac{b}{2}\right) - v\left(-\frac{h}{2},0\right) = \frac{3\nu_b b F(w) L}{2Eh^3} \tag{24}$$

where $b = 4.4$ mm, $L = 50$ mm, $E = 206$ GPa, $\nu_b = 0.3$ and $h = 5$ mm. The total contribution to the separation w is 2η. The quotient $2\eta/w$, given in Fig. 18, is a measure of the error due to anticlastic bending. It can concluded that it is possible to neglect the influence of anticlastic bending.

The second and fourth requirements are less easy to check. These are tested using finite element simulations of the experiments; this is the subject of the following sections.

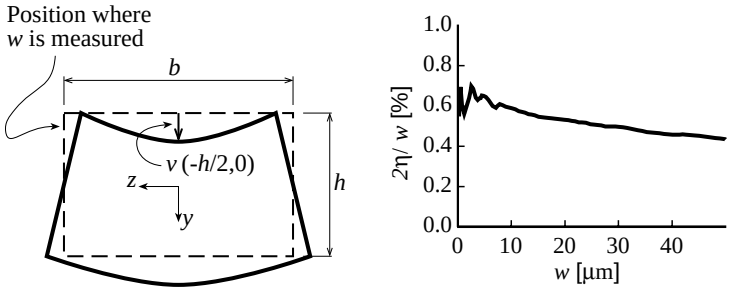

Fig. 18. Left: Anticlastic bending of the cross section of the lower beam. Right: Relative error due to measurement of elongation of the adhesive layer at the outer surface.

5.1. Numerical method

The finite element method is used to simulate the experiments. In these simulations we make use of the commercial program ABAQUS ver. 5.8. The relatively small peel stress σ_0 that affects the adherends suggests that the adherends can be modelled using two node beam elements. Here we use the beam element type B23. This element is based on Euler–Bernoulli beam theory. Consistent with the assumption of a σ–w relation the non-linear elastic spring element, SPRING1 is used to model the adhesive layer. Due to the symmetry, only the upper adherend is modelled. The total length of the specimen is 115 mm and the unbonded length L is set to 78 mm for the specimens of Set 1 and 50 mm for Set 2. These values differ somewhat from the true ones, cf. Table 1. The width, b, is 5 mm for Set 1 and 4.4 mm for Set 2. Furthermore, the height of the adherends is 4.5 mm for Set 1 and 5 mm for Set 2. The adherends are made of steel with the yield strength larger than 470 MPa. Appropriate values of Young's modulus and Poisson's ratio for the steel adherends are 206 GPa and 0.3 respectively. To simplify the input of data and the interpretation of the results, all spring elements are located equidistantly along the specimen. All spring elements, except the first, have the same force–elongation relation given by $F(w) = \sigma(w)bl_e$ where l_e is the distance between the spring elements. The first spring element only represents the action of the adhesive element to the right of the node. This element has the force-elongation relation $F_{\text{first}}(w) = \sigma(w)bl_e/2$. To describe the σ–w curve, two linear segments are used to describe the first two parts. Between two to five segments are used to describe the descending part. The chosen number of segments depends on the curvature of the curve.

The length of the beam elements, l_e, is chosen small enough to accurately capture the gradients of the displacement field. Results from use of an exact analytic solution (Stigh, 1987) indicates that a length of about 0.2 mm should be enough. However, the model is very simple, therefore we finally chose 1000 beam elements. This results in an element length of $l_e = 0.115$ mm. Consequently, in Set 2 there are 566 spring elements in the mesh. As in the experiments, a simulation consists of a monotonically increasing displacement of the loading point.

5.2. Results of simulation

Fig. 19 shows the experimental and simulated F–Δ curves. The curves from Set 1 show a fairly good agreement between the experimental (solid) curve and the simulated (dashed) curve. The slopes of the two curves agree well at the beginning, but at a displacement of about 1 mm the two curves diverge. In the experiment the maximum force is obtained at $\Delta \approx 3.4$ mm whereas it is obtained at $\Delta \approx 3.6$ mm in the simulation. However, the value of the maximum force is practically the same. The curves from Set 2 vir-

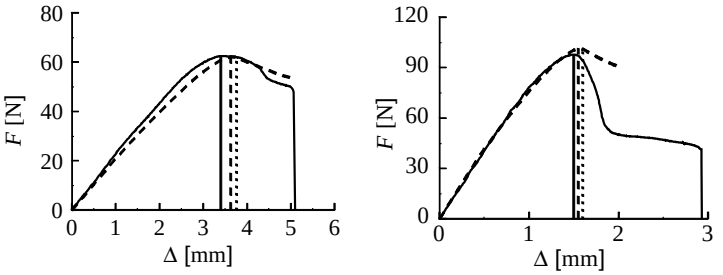

Fig. 19. Experimental (solid line) and simulated (dashed line) F–Δ curves. Left: Specimen from Set 1. Right: Specimen from Set 2. Vertical lines indicates: maximum value of F according to experiment (solid line); maximum value according to simulation (dashed line); and crack propagation according to the simulation (dotted line).

tually coincide until the maximum force is obtained. The maximum force is obtained at almost the same value for the two curves, $\Delta \approx 1.5$ mm. The dotted lines indicate at which displacement a crack, according to the simulation, starts to develop in the adhesive layer, this point is always to the right of the point of the maximum force.

In Fig. 20 the experimental and the simulated θ–Δ curves are shown. The simulation, taken from Set 1, shows very good agreement with the experiment. However, Set 2 shows less good agreement between the experiment and the simulation.

The J–Δ curves, displayed in Fig. 21, show a satisfying agreement between the experiments and the simulations up to the maximum value of J. From this point, the simulations give a constant J. This is a result of using a unique σ–w curve, cf. Eq. (9). However, in the experiments J decreases after a crack has developed.

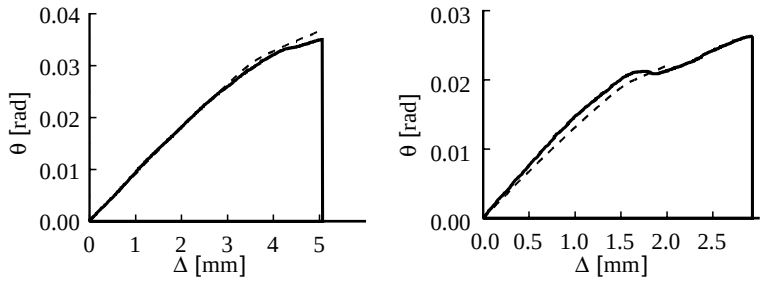

Fig. 20. Experimental (solid line) and simulated (dashed line) θ–Δ curves. Left: Specimen from Set 1. Right: Specimen from Set 2.

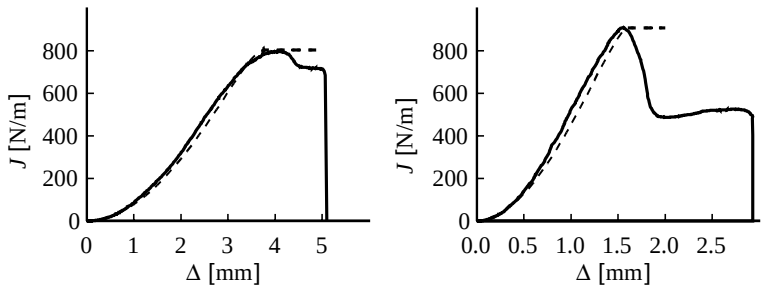

Fig. 21. Experimental (solid line) and simulated (dashed line) J–Δ curves. Left: Specimen from Set 1. Right: Specimen from Set 2.

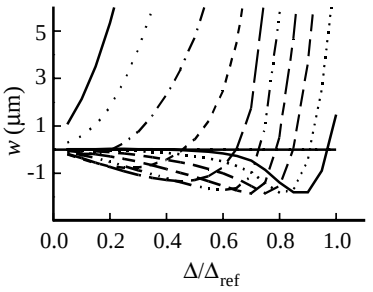

Fig. 22. Elongation of different elements along the adhesive layer w vs. Δ/Δ_{ref} during an experiment. Δ_{ref} corresponds to crack initiation.

It should be observed that the results of the simulations are sensitive to the length L. Although the final part of the σ–w curve is not measured, the simulations show that it is possible to re-create the experiments both qualitatively and quantitatively, thus supporting the extrapolation made in the curve fitting procedure.

The proposed method rests on the assumption of a unique σ–w relation for the adhesive layer. If unloading from a non-elastically deformed state takes place, the proposed method fails since the path at unloading differs from that at loading. However, if the adhesive experiences monotonically increasing or decreasing elongation during an experiment then the difference between a unique σ–w curve and the true one is without significance.

Fig. 22 shows the elongation of the adhesive at consecutive points along the adhesive layer, the distance between the points is 2.3 mm. The first curve shows the elongation at the start of the layer. This part of the adhesive experiences a monotonically increasing elongation, as should be expected. Elements of the adhesive further inside the layer first experiences a compression, later followed by an elongation. The initial compression is understood from the well-known solution for a beam on an elastic foundation.

The maximum compression of any element of the layer does not exceed 2 μm which corresponds to $\sigma = -19.3$ MPa. Moreover, the elastic limit in compression is probably larger than that in tension. Thus, no inelastic deformation is expected at any part of the layer before it starts to elongate. Moreover, no element of the adhesive experiences unloading from an elongated state before a crack starts to propagate. Thus, the use of a unique stress–elongation relation in the theoretical basis for the method is consistent with the results of the simulations.

The forth requirement stated above, namely the sufficiency of a local theory, is less easy to validate. However, the good agreement between the simulated and experimental results indicates that the present ''adhesive layer'' approach is sufficient.

To complete a validation, the possibility to use experimentally obtained relations on other structural configurations should be tested. A numerical analysis should anticipate the behaviour of the structure and onset of fracture. However, one should be careful. It is important to choose the structure with care. The specimen should be chosen such that the shape of the stress–elongation law has a substantial influence on the structural behaviour. This is not the case for many configurations. For instance, the structural behaviour of a DCB-specimen is accurately governed by the properties of the adherends and J_c of the adhesive layer if L is large enough.

6. Conclusions and discussion

In this paper the σ–w curve for an epoxy adhesive has been determined by use of equilibrium of energetic forces. The results have been verified numerically using FE simulations. The agreement between the ex-

periments and the simulations is good. The results show that the constitutive law for the adhesive can be described by an initial linear part followed by a constant part and an ending descending part. Two sets of specimens with different geometries were tested. The specimens in Set 1, which fractured cohesively, were found to be stronger than the specimens in Set 2, which fractured adhesively. The mean value of the maximum tensile strength is about 25 MPa for Set 1 but only about 20 MPa for Set 2. Compared to ordinary bulk tests the maximum tensile strength is found to be 20% lower for Set 1 and 35% lower for Set 2. The mean value of the fracture energy was found to be 820 J/m^2 for Set 1 and 760 J/m^2 for Set 2. It is believed that there are at least two possible reasons for the diverging values between the two sets.

(1) For Set 2 the interface strength between the adherend and the adhesive is weaker than the strength of the adhesive.
(2) As the two sets are manufactured at different times it is possible that the residual stresses are different in the two sets.

The proposed method rests upon assuming a constant adhesive thickness. This is clearly not the case in these experiments though the good agreement between the simulations and experiments indicates that the effect is negligible. In order to validate the method, further experiments must be performed with different geometries. Such experiments are now planned. In these experiments we will change the method to measure w in order to capture the complete σ–w curve. An advantage with the present method is that the σ–w curve is determined from a limited number of measurable quantities, e.g., the present method requires only the width of the adherends. The method also comprises a simple load case. The σ–w curve can easily be implemented into any commercial FE-program using cohesive elements to simulate adhesive joints in structural analysis. It should be recognised that a complete constitutive description of an adhesive layer must also incorporate models of the behaviour at unloading and the effect of mixed peel-shear loading. A numerical method to achieve this is developed by Cannmo et al. (1995). Complementing the present work, Alfredsson (2003a,b) and Alfredsson et al. (2003) develop a method to measure the stress–deformation relation in shear. This curve appears to be an enlarged version of the peel curve.

It might appear even simpler to determine the curve using the butt joint. This would, however, require a very stiff tensile test machine to catch the descending part of the curve. The descending part is important since it determines the conditions at crack propagation. Moreover, testing of but joints requires very careful preparation of the specimen and testing machine to secure rotational symmetry.

It should be recognised that the present σ–w curve is not a material law in the conventional sense, i.e. it is not expected to be independent of all structural features. Specifically, the present constitutive law is expected to depend on the thickness of the layer. It may also depend on other factors, e.g. on the adherends, the loading rate and the residual stresses. How these factors influence the constitutive law remains to be determined. However, it is reasonable to assume that the present law should be applicable to different structures as long as the thickness and the manufacturing process of the adhesive layer remain the same.

Acknowledgements

Support from AB Volvo and Chalmers University of Technology are gratefully acknowledged.

References

Adams, R.D., Coppendale, J., Peppiatt, N.A., 1978. Stress analysis of axisymmetric butt joints loaded in torsion and tension. Journal of Strain Analysis 13, 1–10.

Adams, R.D., Coppendale, J., 1979. The stress–strain behaviour of axially-loaded butt joints. Journal of adhesion 10, 49–62.

Alfredsson, K.S., 2003a. On the energy release rate of the end-notch flexure adhesive joint specimen, submitted for publication.

Alfredsson, K.S., 2003b. On the determination of constitutive properties of adhesive layers loaded in shear—an inverse solution. International Journal of Fracture, in press.

Alfredsson, K.S., Biel, A., Leffler, K., 2003. An experimental method to determine the complete stress–elongation relation for a structural adhesive layer loaded in shear. In: Proceedings of 9th International Conference on the Mechanical Behaviour of Materials.

Alfredsson, K.S., Stigh, U., 2003. Deterioration and healing of thermoelastoplastic material models—a thermodynamically based framework for continuum damage mechanics, submitted for publication.

Andersson, T., 2002. Stress–elongation behaviour of adhesive layers—an experimental method. Thesis for the degree of licentiate in engineering. Department of Applied Mechanics, Chalmers University of Technology, Göteborg, Sweden.

Andersson, T., Stigh, U., 2001. Verification of an experimental method to measure the stress–elongation law for an adhesive layer using a DCB-specimen. In: Ravi-Chandar, B.L. et al. (Eds.), Proceedings of 10th International Conference on Fracture. In: Advances in Fracture Research. Elsevier.

Cannmo, P., Runesson, K., Ritsinmaa, M., 1995. Modelling of plasticity and damage in a polycrystalline microstructure. International Journal of Plasticity 11, 949–970.

Chai, H., 1988. Shear fracture. International Journal of Fracture 37, 137–159.

Edlund, U., 1992. Mechanical analysis of adhesive joints: models and computational methods. Linköping Studies in Science and Technology, Dissertation No. 291, Linköping University, Linköping, Sweden.

Eshelby, J.D., 1951. The force on an elastic singularity. Philosophical Transactions of the Royal Society of London Series A 244, 87–112.

Fernberg, S.P., Berglund, L.A., 2001. Bridging law and toughness characterisation of CSM and SMC composites. Composites Science and Technology 61, 2445–2454.

Jacobsen, T.K., Sørensen, B.F., 2001. Mode I intra-laminar crack growth in composites—modelling of R-curves from measured bridging laws. Composites Part A 32, 1–11.

Klarbring, A., 1991. Derivation of a model of adhesively bonded joints by the asymptotic expansion method. International Journal of Engineering Science 29 (4), 493–512.

Nairn, J.A., 2000. Energy release rate analysis for adhesive and laminate double cantilever beam specimens emphasizing the effect of residual stresses. International Journal of Adhesion and Adhesives 20, 59–70.

Olsson, P., Stigh, U., 1989. On the determination of the constitutive properties of thin interphase layers—an exact solution. International Journal of Fracture 41, R71–R76.

Sharpe, W.N., Jr., 1989. An interferometric strain/displacement measurement system. NASA Technical Memorandum 101638, Langley Research center, Virginia.

Stigh, U., 1987. Initiation and growth of an interface crack. In: Verchery, G., Cardon, A.H. (Eds.), Proceeding of the European Mechanics Colloquium 227. In: Mechanical Behaviour of Adhesive Joints. Pluralis, Paris, pp. 237–248.

Stigh, U., 1988. Damage and crack growth analysis of the double cantilever beam specimen. International Journal of Fracture 37, R13–R18.

Stigh, U., Andersson, T., 2000. An experimental method to determine the stress–elongation relation for a structural adhesive layer loaded in peel. In: Williams, J.G., Pavan, A. (Eds.), Proceedings of the second ESIS Conference. In: Fracture of Polymers, Composites and Adhesives, ESIS publication 27. Elsevier, Amsterdam, pp. 297–306.

Sørensen, B.F., 2002. Cohesive law and notch sensitivity of adhesive joints. Acta. Materialia 50, 1053–1061.

Sørensen, B.F., Jacobsen, T.K., 1998. Large-scale bridging in composites: R-curves and bridging laws. Composites Part A 29A, 1443–1451.

Timoshenko, S.P., Goodier, J.N., 1970. Theory of Elasticity. McGraw-Hill, Singapore.

Wernersson, H., Gustafsson, P.J., 1987. The complete stress–slip curve of wood-adhesive in pure shear. In: Verchery, G., Cardon, A.H. (Eds.), Proceeding of the European Mechanics Colloquium 227. In: Mechanical Behaviour of Adhesive Joints. Pluralism, Paris, pp. 139–150.

Xia, Z.C., Hutchinson, J.W., 1994. International Journal of Solids and Structures 8, 1133–1148.

Yang, Q.D., Thouless, M.D., Ward, S.M., 1999. Numerical simulations of adhesively-bonded beams failing with extensive plastic deformation. Journal of the Mechanics and Physics of Solids 47, 1337–1353.

Yang, Q.D., Thouless, M.D., Ward, S.M., 2001a. Elastic-plastic mode-II fracture of adhesive joints. International Journal of Solids and Structures 38, 3251–3262.

Yang, Q.D., Thouless, M.D., Ward, S.M., 2001b. Mixed-mode fracture analyses of plastically-deforming adhesive joints. International Journal of Fracture 110, 175–187.